Polydispersity Effects in Dilute Polymer Solutions in the Good-Solvent Regime

Andrea Pelissetto*

Dipartimento di Fisica and INFN-Sezione di Roma I, Università degli Studi di Roma "La Sapienza", Piazzale Moro 2, I-00185 Roma, Italy

Received February 1, 2006; Revised Manuscript Received April 7, 2006

ABSTRACT: We study the behavior of dilute polydisperse polymer solutions in the good-solvent regime. We compute the second virial coefficient for polymers of different degree of polymerization and for general polydispersity distributions. We also determine the effective center-of-mass pair potential for polymers of different length. These results, combined with the integral-equation formalism and the hypernetted-chain closure, allow us to determine the osmotic pressure and the intermolecular structure function in the dilute regime for general polydispersity distributions.

1. Introduction

In the limit of a large number of monomers, polymers show a universal scaling behavior.[1−3] Indeed, global polymer properties can be characterized in terms of exponents and dimensionless ratios that do not depend on chemical details on a molecular scale. Many theoretical works considered the behavior of monodisperse solutions: all chains have the same number of monomers. However, from the experimental point of view, it is of interest to discuss the effects of polydispersity, i.e., solutions of polymers of different length. In this paper we consider polymer solutions in the good-solvent regime, i.e., above the θ-temperature. In this regime chains are swollen, and the typical size of the polymer scales as L^{ν}, where L is the number of monomers (degree of polymerization) and ν is a universal exponent,[4] $\nu \approx 0.5876$.

We first consider the zero-density limit. We determine the second virial coefficient $B_2(L_1,L_2)$ for two polymers of length L_1 and L_2 and the corresponding effective pair potential $\beta v_2(r;L_1,L_2)$. Since we focus on universal properties, we can use any model that captures the basic properties of polymer behavior. For this purpose we consider self-avoiding walks on a cubic lattice. Once $B_2(L_1,L_2)$ is known, we are able to compute the first density correction to the compressibility factor $Z \equiv \beta\Pi/\rho$, where Π is the osmotic pressure and ρ is the density, and to the zero-momentum structure function for different polydispersity distributions.

Knowledge of the zero-density pair potential allows us to study polymer solutions in the dilute regime. For this purpose, we consider the coarse-grained fluid model in which polymers are replaced by point particles interacting by means of the zero-density coarse-grained pair potential (see refs 5−7 and references therein). This approach should be accurate in the dilute regime in which the effect of the neglected three- and higher-order interactions that arise in the coarse-grained procedure is small.[8] To determine the thermodynamic properties of the fluid, we use the integral-equation formalism.[9] In particular, we employ the hypernetted-chain (HNC) closure, which has been shown to be extremely accurate for soft-core potentials.[10] We focus on the osmotic pressure and on the intermolecular structure factor that are determined for solutions in which there are two polymer species with different degree of polymerization (we call them bimodal solutions) and for solutions with Schultz polydispersity distribution. All calculations refer to the good-solvent regime. The crossover toward the θ point will be the object of a forthcoming publication.

The paper is organized as follows. In section 2 we define our model and give the definitions of the quantities we compute. In section 3 we determine the universal scaling function for the second virial coefficient and for the effective pair potential for polymers of different length. In section 4 we determine the compressibility factor Z and the intermolecular structure factor in the dilute limit for several polydispersity distributions. In section 5 we present our conclusions.

2. Definitions

Since we are interested in universal polymer properties, we can consider any model that captures the basic physical properties of the polymeric system. We consider the well-known self-avoiding walk (SAW) model on a cubic lattice with attraction; i.e., we introduce an effective attraction $-\epsilon$ between nonconnected nearest-neighbor monomers. If $\beta \equiv -\epsilon/k_B T$ is the dimensionless inverse temperature, the statistical properties depend in general on β and on the chain length L. However, for $\beta < \beta_\theta$—β_θ is the inverse θ temperature, $\beta_\theta \approx 0.269$ in the present model[11]—the scaling limit $L \to \infty$ is β independent, in the sense that dimensionless functions and exponents do not depend on β. As we discuss below, we shall use the β dependence at finite L to determine "optimal" quantities that show a faster convergence to the scaling limit.

We perform a Monte Carlo simulation of isolated SAWs (zero-density limit) using the pivot algorithm[12−15] and measure the following quantities:

(1) the radius of gyration of a polymer of length L:

$$R_g^2(L;\beta) \equiv \frac{1}{2(L+1)^2}\sum_{i,j}\langle(\mathbf{r}_i - \mathbf{r}_j)^2\rangle \qquad (1)$$

where the sums go over the $L+1$ sites of the chain and $\mathbf{r}_i$ is the corresponding position.

(2) the second virial coefficient for two polymers of length L_1 and L_2:

* E-mail: andrea.pelissetto@roma1.infn.it.

10.1021/ma060250l CCC: $33.50
Published on Web 05/10/2006

$$B_2(L_1,L_2;\beta) \equiv \frac{1}{2}\int \mathrm{d}^3\,\mathbf{r}_1\,\langle 1 - \mathrm{e}^{-\beta H(1,2)}\rangle_{0,\mathbf{r}_1} \qquad (2)$$

where the average is over two walks of length L_1 and L_2, the first one starting at the origin and the second at $\mathbf{r}_1$; $H(1,2)$ is their interaction energy.

(3) the effective pair potential between the centers of mass of two polymers:

$$\beta v_2(r;L_1,L_2;\beta) \equiv -\ln\langle \mathrm{e}^{-\beta H(1,2)}\rangle_r \qquad (3)$$

where $H(1,2)$ is the interaction energy between the two SAWs and the average is taken over pairs of walks of length L_1 and L_2 such that the distance between their centers of mass is r.

(4) the effective three-body potential between the centers of mass of three polymers of length L_1, L_2, and L_3:

$$\beta v_3(r_{12},r_{13},r_{23};L_1,L_2,L_3;\beta) \equiv -\ln\left(\frac{\langle \mathrm{e}^{-\beta H(1,2)-\beta H(1,3)-\beta H(2,3)}\rangle_{r_{12},r_{13},r_{23}}}{\langle \mathrm{e}^{-\beta H(1,2)}\rangle_{r_{12}}\langle \mathrm{e}^{-\beta H(1,3)}\rangle_{r_{13}}\langle \mathrm{e}^{-\beta H(2,3)}\rangle_{r_{23}}}\right) \qquad (4)$$

where r_{ij} is the distance between the centers of mass of walk i and j.

The second virial coefficient is not universal. A universal quantity is obtained by considering the following dimensionless ratio:

$$A_2(L_1,L_2;\beta) \equiv \frac{B_2(L_1,L_2;\beta)}{R_g(L_1;\beta)^{3/2}R_g(L_2;\beta)^{3/2}} \qquad (5)$$

where $R_g(L;\beta)$ is the gyration radius at zero density.

According to the renormalization group, in the good-solvent regime any zero-density universal ratio $\mathscr{R}$ that is a function of L_1 and L_2 scales as[16]

$$\mathscr{R}(L_1,L_2;\beta) = \mathscr{R}^*(\lambda) + a_{\mathscr{R}}(\beta) f_{\mathscr{R}}(\lambda)(L_1L_2)^{-\Delta/2} + \ldots \qquad (6)$$

with $\lambda \equiv L_1/L_2$ and $f_{\mathscr{R}}(1) = 1$ (normalization condition). The leading function $\mathscr{R}^*(\lambda)$ is universal as well as the correction-to-scaling function $f_{\mathscr{R}}(\lambda)$ and the exponent Δ. On the other hand, the coefficient $a_{\mathscr{R}}(\beta)$ is model dependent. Since Δ is quite small,[17] $\Delta = 0.515 \pm 0.007^{+0.010}_{-0.000}$, scaling corrections are usually the main source of error in high-precision estimates of polymer universal properties. There are, however, a few methods that allow us to obtain more precise estimates. One possibility is to use the β dependence of $a_{\mathscr{R}}(\beta)$ and work at $\beta = \beta^{\mathrm{opt}}$, where β^{opt} is such that $a_{\mathscr{R}}(\beta^{\mathrm{opt}}) = 0$. The value β^{opt} satisfies an important property: it does not depend on the observable $\mathscr{R}$. For the SAW model on a cubic lattice[18] $\beta^{\mathrm{opt}} \approx 0.054$. Another possibility,[18] which will also be used here, consists of performing simulations at two values of β, β_1 and β_2, and consider the combination

$$\mathscr{R}_{\mathrm{opt}} = p\mathscr{R}(\beta_1) + (1-p)\mathscr{R}(\beta_2) \qquad (7)$$

In general, there is a an observable-independent value, p_{opt}, such that $\mathscr{R}_{\mathrm{opt}}$ does not have leading scaling corrections. For the SAW model,[18] if $\beta_1 = 0$ and $\beta_2 = 0.1$, $p_{\mathrm{opt}} = 0.46 \pm 0.04$.

The pair potential shows a scaling behavior analogous to that given in eq 6:

$$\beta v_2(r;L_1,L_2;\beta) = v_\infty(\xi;\lambda) + a_v(\beta) v_c(\xi;\lambda)(L_1L_2)^{-\Delta} + \ldots \qquad (8)$$

with $\lambda \equiv L_1/L_2$ and $v_c(0;1) = 1$ (normalization condition). The quantity ξ is a dimensionless length scale: $\xi \equiv r/R_s$. The scale R_s is completely arbitrary. Any choice is equally good as long as R_s is a quantity that is related to the global size of at least one of the two polymers. We choose

$$R_s^2(L_1,L_2) = \frac{1}{2}[R_g^2(L_1) + R_g^2(L_2)] \qquad (9)$$

The function $A_2^*(\lambda)$ satisfies several relations. First, since $A_2(L_1,L_2;\beta)$ is symmetric under the interchange of L_1 and L_2, we have $A_2^*(\lambda) = A_2^*(1/\lambda)$. Second, the second virial coefficient satisfies the de Gennes[19] relation $B_2(L_1,L_2) \sim L_1L_2^{3\nu-1}$ for $L_1/L_2 \to \infty$. It implies

$$A_2^*(\lambda) \sim \lambda^{1-3\nu/2} \sim \lambda^{0.1188}, \quad \text{for } \lambda \to \infty$$
$$A_2^*(\lambda) \sim \lambda^{3\nu/2-1} \sim \lambda^{-0.1188}, \quad \text{for } \lambda \to 0 \qquad (10)$$

A similar relation can be derived for $v_\infty(\xi;\lambda)$. Indeed, $A_2^*(\lambda)$ and $v_\infty(\xi;\lambda)$ are related by

$$A_2^*(\lambda) = 2^{1/2}\pi\lambda^{-3\nu/2}(1+\lambda^{2\nu})^{3/2}\int_0^\infty \mathrm{d}\xi\,\xi^2[1 - e^{-v_\infty(\xi;\lambda)}] \qquad (11)$$

For $\lambda \to 0$ the pair potential must go to zero. Indeed, in the scaling limit the polymer behavior does not depend on the solvent properties: in other words, the presence of molecules that are small compared to the polymer size does not change the universal properties of the polymer unless it drives the solution into the poor-solvent regime. In the limit $\lambda \to 0$, the solution can be represented as a solution of long polymers in which short polymers are also considered as part of the solvent. Thus, at the coarse-grained scale, one should only consider the interactions among long polymers, implying that the pair potential between a long and a short polymer is zero. Thus, for $\lambda \to 0$, we have

$$A_2^*(\lambda) \approx 2^{1/2}\pi\lambda^{-3\nu/2}\int_0^\infty \mathrm{d}\xi\,\xi^2 v_\infty(\xi;\lambda) \qquad (12)$$

We shall see below that the effective pair potential is strictly positive. Thus, by using eq 10, we obtain for $\lambda \to 0$ the relation

$$v_\infty(\xi;\lambda) \approx \lambda^{3\nu-1} v_0(\xi) \qquad (13)$$

where $v_0(\xi)$ is a positive function. Such a relation gives the rate by which the effective pair potential vanishes as $\lambda \to 0$.

Knowledge of $A_2^*(\lambda)$ allows us to determine the low-density behavior of the osmotic pressure Π and of the density correlation function $S(\mathbf{q})$ at $\mathbf{q} = 0$ for a general polydispersity distribution. We assume that the polymer solution contains polymers of different length L with distribution $P(L)$. We assume the distribution to be normalized so that

$$\sum_L P(L) = 1, \quad \sum_L LP(L) = N \qquad (14)$$

where N is the average polymer length. For small densities the osmotic pressure behaves as

$$\frac{\beta\Pi}{\rho} = 1 + B_2^\Pi(P)\rho + O(\rho^2) \qquad (15)$$

where

$$B_2^\Pi(P) = \sum_{L_1,L_2} P(L_1)\,P(L_2)\,B_2(L_1,L_2) \qquad (16)$$

and ρ is the polymer number density. Note that in experimental

work one defines a different virial coefficient by writing[20]

$$\frac{\Pi}{\rho_w RT} = \frac{1}{M_n} + B_{2,expt}^{\Pi}\rho_w + O(\rho_w^2) \tag{17}$$

where ρ_w is the ponderal polymer concentration and M_n is the number-averaged molecular weight, $M_n \equiv mNN_A$, m being the mass of a single monomer and N_A the Avogadro number. The two quantities are related by

$$B_{2,expt}^{\Pi} = \frac{N_A B_2^{\Pi}(P)}{M_n^2} \tag{18}$$

For the analysis of scattering data the relevant quantity is the density correlation function:

$$S(\mathbf{q}) \equiv \int d^3\,\mathbf{r} e^{i\mathbf{q}\cdot\mathbf{r}} \langle (c(\mathbf{r}) - c)(c(0) - c)\rangle \tag{19}$$

where $c(\mathbf{r})$ is the local monomer concentration and c its average. For $\mathbf{q} = 0$ we have (see ref 3, eq A 15.10)

$$\frac{S(\mathbf{0})}{\rho \sum_L L^2 P(L)} = 1 - 2\rho B_2^S + O(\rho^2) \tag{20}$$

where

$$B_2^S(P) = \frac{\sum_{L_1,L_2} L_1 L_2 P(L_1)\, P(L_2)\, B_2(L_1,L_2)}{\sum_L L^2 P(L)} \tag{21}$$

For a monodisperse solution $B_2^S = B_2^{\Pi} = B_2(L,L)$. The virial coefficient $B_2^S(P)$ can be related to that used in experimental work. There, one usually considers the scattering intensity I_0 at zero scattering angle that has an expansion of the form[20]

$$\frac{K\rho_w}{I_0} = \frac{1}{M_w} + 2B_{2,expt}^{S}\rho_w + O(\rho_w^2) \tag{22}$$

where K is a constant and M_w is the weight-averaged molecular mass, $M_w = mN_A\sum_L L^2 P(L)/N$.

Since $I_0 \propto S(0)$, it is easy to derive the relation

$$B_{2,expt}^{S} = \frac{N_A B_2^S(P)}{M_n M_w} \tag{23}$$

Finally, we consider the intramolecular form factor

$$F(\mathbf{q}) \equiv \frac{1}{N_{mon}} \sum_m \sum_{ab} \langle e^{i\mathbf{q}\cdot(\mathbf{r}_a^{(m)} - \mathbf{r}_b^{(m)})}\rangle \tag{24}$$

where m labels the polymers present in the solution, $\mathbf{r}_a^{(m)}$ is the position of monomer a belonging to polymer m, and N_{mon} is the total number of monomers. For $\mathbf{q} \to 0$ we have

$$F(\mathbf{q}) = 1 - \frac{q^2}{3} R_{g,Z}^2(P) + O(q^4) \tag{25}$$

where

$$R_{g,Z}^2(P) = \frac{\sum_L L^2 P(L) R_g^2(L)}{\sum_L L^2 P(L)} \tag{26}$$

is the so-called Z-average of the radius of gyration. Since this quantity is directly accessible experimentally, we will use $R_{g,Z}(P)$ at zero density as a measure of the average polymer size. As before, we consider the invariant ratios

$$A_2^{\Pi}(P) = \frac{B_2^{\Pi}(P)}{R_{g,Z}^3(P)} \tag{27}$$

$$A_2^{S}(P) = \frac{B_2^{S}(P)}{R_{g,Z}^3(P)} \tag{28}$$

where the gyration radii are computed at zero density. In the case of polydisperse systems the scaling limit corresponds to $N \to \infty$. Moreover, we must assume that the polydispersity distribution assumes a scale-invariant form

$$P(L) = \frac{1}{N} p(L/N) \tag{29}$$

with

$$\int dy\, p(y) = 1, \quad \int dy\, y p(y) = 1 \tag{30}$$

Then, in the scaling limit $N \to \infty$ we obtain the relations

$$A_2^{\Pi}(P) = \frac{\mathcal{N}_2^{3/2}}{\mathcal{N}_1^{3/2}} \int dy\, dz\, p(y)p(z)(yz)^{3\nu/2} A_2^*(y/z)$$

$$A_2^{S}(P) = \frac{\mathcal{N}_2^{1/2}}{\mathcal{N}_1^{3/2}} \int dy\, dz\, p(y)p(z)(yz)^{3\nu/2+1} A_2^*(y/z)$$

$$\mathcal{N}_1 = \int dy\, y^{2+2\nu} p(y)$$

$$\mathcal{N}_2 = \int dy\, y^2 p(y) \tag{31}$$

A realistic distribution is the Schultz distribution. It depends on a parameter σ and is explicitly given by

$$p(y;\sigma) = \frac{\sigma^\sigma}{\Gamma(\sigma)} y^{\sigma-1} e^{-\sigma y} \tag{32}$$

In this case we obtain

$$A_2^{\Pi}(\sigma) = \frac{(\sigma+1)^{3/2}\sigma^2\Gamma(2\sigma+3\nu)}{\Gamma(\sigma+1)^{1/2}\Gamma(\sigma+2\nu+2)^{3/2}} \int_0^1 d\mu\, [\mu(1-\mu)]^{\sigma+3\nu/2-1} A_2^*(\mu/(1-\mu)) \tag{33}$$

$$A_2^{S}(\sigma) = \frac{(\sigma+1)^{1/2}\sigma\Gamma(2\sigma+3\nu+2)}{\Gamma(\sigma+1)^{1/2}\Gamma(\sigma+2\nu+2)^{3/2}} \int_0^1 d\mu\, [\mu(1-\mu)]^{\sigma+3\nu/2} A_2^*(\mu/(1-\mu)) \tag{34}$$

We also determine the virial coefficients for a bimodal distribution, i.e., for the ternary system in which there are two polymer species with the same chemical composition but with different lengths L_1 and L_2:

$$p(y) = \alpha\delta(y - y_1) + (1 - \alpha)\delta(y - y_2), \quad y_i \equiv L_i/N \tag{35}$$

where $N = \alpha L_1 + (1 - \alpha)L_2$. Setting $\lambda = y_2/y_1 = L_2/L_1$ and $\beta = 1 - \alpha$, we find

$$A_2^{\Pi}(\alpha,\lambda) = \frac{(\alpha + \beta\lambda^2)^{3/2}[(\alpha^2 + \beta^2\lambda^{3\nu})A_2{}^*(1) + 2\alpha\beta\lambda^{3\nu/2}A_2{}^*(\lambda)]}{(\alpha + \beta\lambda^{2+2\nu})^{3/2}} \tag{36}$$

$$A_2^{S}(\alpha,\lambda) = \frac{(\alpha + \beta\lambda^2)^{1/2}[(\alpha^2 + \beta^2\lambda^{2+3\nu})A_2{}^*(1) + 2\alpha\beta\lambda^{1+3\nu/2}A_2{}^*(\lambda)]}{(\alpha + \beta\lambda^{2+2\nu})^{3/2}} \tag{37}$$

It is also interesting to consider the following quantity that does not contain any length scale and is easily accessible experimentally:[3,21]

$$R_2^{S}(\alpha,\lambda) \equiv \frac{B_{2,\mathrm{expt}}^{S}(P)}{B_{2,\mathrm{expt}}(L_1,L_1)} = \frac{L_1{}^2 B_2^{S}(P)}{(\alpha L_1{}^2 + \beta L_2{}^2)B_2(L_1,L_1)} \tag{38}$$

For this quantity we obtain

$$R_2^{S}(\alpha,\lambda) = \frac{(\alpha^2 + \beta^2\lambda^{2+3\nu})A_2{}^*(1) + 2\alpha\beta\lambda^{1+3\nu/2}A_2{}^*(\lambda)}{A_2{}^*(1)(\alpha + \beta\lambda^2)^2} \tag{39}$$

3. Zero-Density Results

We have performed an extensive set of simulations for $\beta = 0.0$ and $\beta = 0.1$, considering SAWs of length L varying between 50 and 16 000. We have determined $A_2(L_1,L_2;\beta)$ and $\beta\upsilon_2(r;L_1,L_2;\beta)$ for 321 pairs of L_1 and L_2 ($L_1 < L_2$), considering ratios λ as small as 0.006 25. We used the pivot algorithm to generate the walks[12−15] and the hit-or-miss algorithm to compute the second virial coefficient.[22]

The results for $A_2(L_1,L_2;\beta)$ for $\beta = 0$ are reported in Figure 1 (top) as a function of λ. Of course, because of the symmetry $\lambda \to 1/\lambda$, we only consider the case $L_1 \le L_2$, i.e., $\lambda \le 1$. As L_1 and L_2 increase, points clearly approach a universal function of λ. Note, however, that there are significant scaling corrections. Faster convergence is observed for the optimal combination (7) which is reported in Figure 1 (bottom). In this case, we use $\beta_1 = 0$, $\beta_2 = 0.1$, and $p_{\mathrm{opt}} = 0.046$. On the scale of the figure, essentially all points collapse on a single curve. We also check the small-λ prediction (10). For this purpose, we consider

$$f(L_1,L_2;\beta) \equiv \left(\frac{L_1L_2}{L_1{}^2 + L_2{}^2}\right)^{1-3\nu/2} A_2(L_1,L_2;\beta) \tag{40}$$

In the scaling limit $f(L_1,L_2;\beta)$ converges to a function $f^*(\lambda)$, such that, if prediction (10) is correct, $f^*(0)$ is finite and nonvanishing. This is indeed observed in Figure 2, where we plot the optimal combination $f_{\mathrm{opt}}(L_1,L_2)$. In this figure, one can appreciate scaling corrections that are clearly less than 1%. The function $f^*(\lambda)$ shows a tiny dependence on λ that can be parametrized by a polynomial in $\mu \equiv \lambda/(1 + \lambda^2)$ (we use this particular combination to ensure the symmetry $\lambda \to 1/\lambda$). A fit constrained to reproduce $A_2{}^*(1) = 5.494$ (ref 18) gives

$$A_2{}^*(\lambda) = \mu^{3\nu/2-1}(a + b\mu + c\mu^2) \tag{41}$$

with $a = 4.611$, $b = 1.153$, and $c = -0.510$. This result can be compared with the renormalization-group predictions.[3,23,24] The

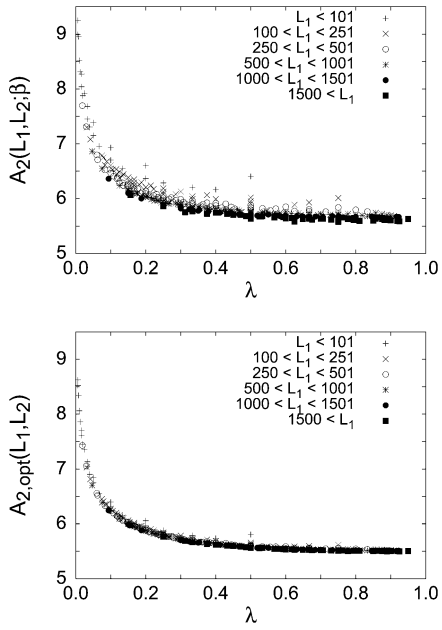

Figure 1. Normalized second virial coefficient as a function of $\lambda \equiv L_1/L_2$. In the upper plot we report the results for $A_2(L_1,L_2;\beta=0)$; in the lower plot we report the optimal combination $A_{2,\mathrm{opt}}(L_1,L_2)$. To identify the scaling corrections, we use different symbols depending on L_1 (the length of the shortest polymer).

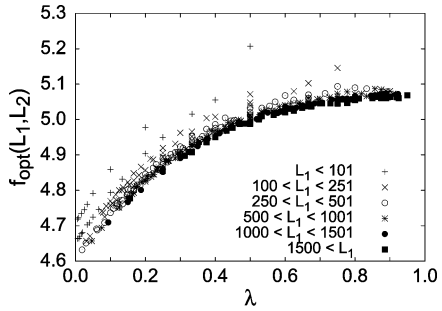

Figure 2. Results for $f_{\mathrm{opt}}(L_1,L_2)$ as a function of $\lambda \equiv L_1/L_2$.

one-loop ϵ expansion gives

$$a = f^*(0) = A^*(1)\left[1 - \frac{\epsilon}{8}(4\ln 2 - 1)\right] \approx 4.28 \tag{42}$$

where we have used the Monte Carlo estimate $A_2{}^*(1) = 5.494$ and we have set $\epsilon = 1$. This is reasonably close to our estimate $f^*(0) \approx 4.61$, the difference being ∼7%. The ratio $f^*(0)/A^*(1)$ has also been determined experimentally. Reference 21 quotes 0.95 ± 0.08, which is in reasonable agreement with our estimate 0.84.

It is difficult to estimate the error on the parametrization (41). An estimate can be obtained by computing the fixed-point value $\bar{g}^*$ of the four-point renormalized coupling used in field-theoretical approaches. With the standard normalization used in field theory, we have[16]

$$\bar{g}^* = \frac{(6R_{\mathrm{ge}})^{3/2}}{\pi} \frac{\Gamma(3\nu + 2\gamma)}{\Gamma(\gamma)^{1/2}\Gamma(\gamma + 2\nu)^{3/2}} \int_0^\infty \mathrm{d}\lambda\, \lambda^{3\nu/2+\gamma-1}(1 + \lambda)^{-3\nu-2\gamma} A_2{}^*(\lambda) \tag{43}$$

where γ is the partition-function critical exponent and $R_{\mathrm{ge}} \equiv R_{\mathrm{g}}{}^2/R_{\mathrm{e}}{}^2$, $R_{\mathrm{e}}{}^2$ being the average squared end-to-end distance. Using[4,25,26] $R_{\mathrm{ge}} = 0.15995 \pm 0.00010$, $\gamma = 1.1575 \pm 0.0006$, and $\nu = 0.5876 \pm 0.0001$, we obtain $\bar{g}^* \approx 1.401$. This is in

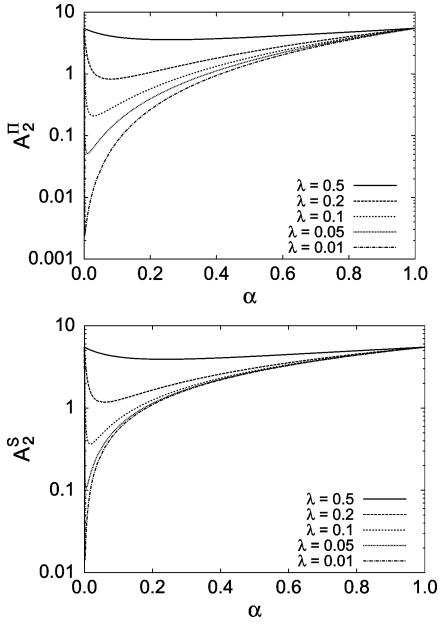

Figure 3. Results for $A_2^{\Pi}(\lambda)$ and $A_2^{S}(\lambda)$ for a bimodal system as a function of the number fraction α of the longest polymer. Here $\lambda = L_2/L_1$.

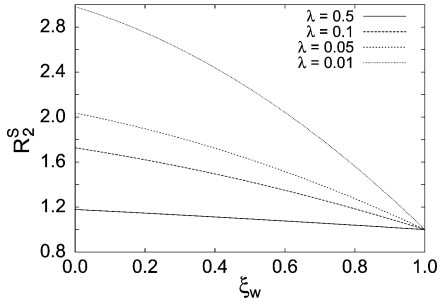

Figure 4. Results for $R_2^{S}(\lambda)$ for a bimodal system as a function of ξ_w. Here $\lambda = L_2/L_1$.

good agreement with the estimates obtained by using field theory and high-temperature expansions,[27−30] $\bar{g}^* = 1.40 \pm 0.01$. The nice agreement indicates that the error should be safely below 1%.

Using the parametrization (41) and the expressions reported in the preceding section, we can compute the second virial coefficient for bimodal systems. In Figure 3 we report $A_2^{\Pi}(\lambda)$ and $A_2^{S}(\lambda)$ as obtained from eqs 36 and 37 as a function of the number fraction α of the polymer of length L_1 for several values of $\lambda \equiv L_2/L_1$. For $\alpha = 0$ and $\alpha = 1$, $A_2^{\Pi} = A_2^{S} = A_2^*(1) \approx 5.494$. For intermediate values these functions become significantly small and have a deep minimum for $\alpha = \alpha_c$ with $\alpha_c \to 0$ as $\lambda \to 0$. In Figure 4 we report $R_2^{S}(\lambda)$ for several values of λ in terms of the variable

$$\xi_w \equiv \frac{\alpha L_1^2}{\alpha L_1^2 + \beta L_2^2} = \frac{\alpha}{\alpha + \beta\lambda^2} \tag{44}$$

This function is in very good agreement with the renormalization-group predictions[3,24] and with experiments:[21] in particular, for each λ it is a decreasing function of ξ_w and does not show a maximum at some intermediate composition, as predicted by Flory-type smoothed density models (see the discussion in refs 3 and 21).

Given $A_2^*(\lambda)$, we can also determine $A_2^{S}(\sigma)$ and $A_2^{\Pi}(\sigma)$ for the Schultz distribution. The results are reported in Figure 5.

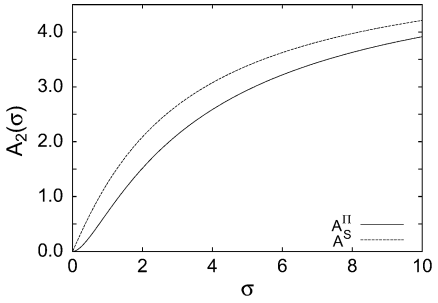

Figure 5. Results for $A_2^{\Pi}(\sigma)$ and $A_2^{S}(\sigma)$ as a function of the Schultz parameter σ.

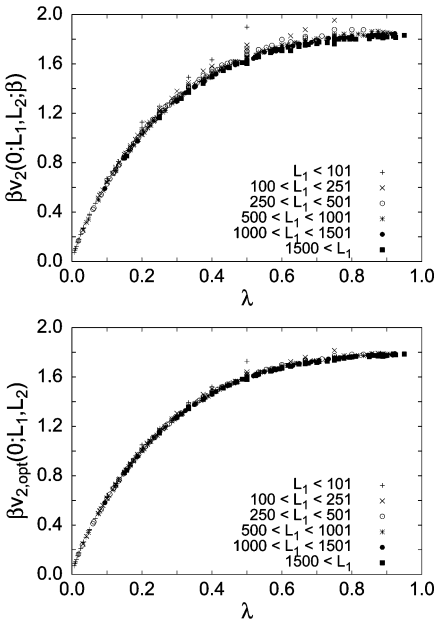

Figure 6. Effective pair potential at full overlap as a function of $\lambda \equiv L_1/L_2$. In the upper plot we report $\beta v_2(r = 0; L_1, L_2; \beta = 0)$ and in the lower plot the optimal combination $\beta v_{2,\mathrm{opt}}(r = 0; L_1, L_2)$.

For $\sigma \to 0$ we obtain $A_2^{S}(\sigma) \approx 1.427\sigma$ and $A_2^{\Pi}(\sigma) \approx 1.935\sigma^2$. For large values of σ, the distribution becomes narrow and centered at 1, so that we recover $A_2(\sigma) \approx A_2^*(1) \approx 5.494$ with corrections of order $1/\sigma$. For $\sigma \gtrsim 30$ a good approximation is

$$A_2^{S}(\sigma) \approx 5.494 - 16.3/\sigma \qquad A_2^{\Pi}(\sigma) \approx 5.494 - 20.5/\sigma \tag{45}$$

For $\sigma = 1$, the case in which $p(x) = e^{-x}$, we obtain $A_2^{S}(1) \approx 1.246$ and $A_2^{\Pi}(1) \approx 0.714$.

The behavior of the pair potential can be derived analogously. In Figure 6 we report the effective pair potential at full overlap ($r = 0$) for $\beta = 0$ (top) and for the optimal combination (bottom). The data collapse on a single curve, as predicted by renormalization group. Also, the asymptotic formula (13) (with $v_0(0) \neq 0$) is well verified. The data are well fitted by the simple formula

$$v_\infty(\xi{=}0;\lambda) = \mu^{0.7628}(a + b\mu + c\mu^2 + d\mu^3) \tag{46}$$

where $a = 3.4147$, $b = 2.3818$, $c = -11.353$, $d = 9.9554$, and $\mu \equiv \lambda/(1 + \lambda^2)$. Renormalization-group predictions have been obtained in ref 31. However, they are very imprecise. At leading order they predict $a = \lim_{\lambda\to 0}\lambda^{1-3\nu} v_\infty(\xi = 0;\lambda) = (9/4 + \sqrt{3}\pi) \approx 7.7$, to be compared with our result $a \approx 3.41$. At one loop, using the results reported in their Figure 3, $\log v_\infty(\xi = 0;\lambda) \approx$

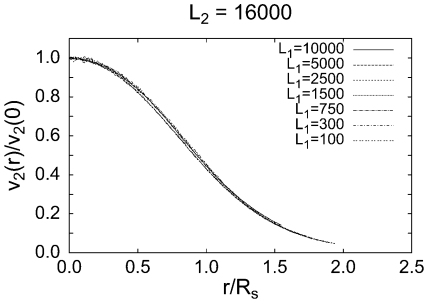

Figure 7. Results for $\beta v_2(r;L_1,L_2;\beta)/\beta v_2(0;L_1,L_2;\beta)$ as a function of $\xi \equiv r/R_s$. Here $L_2 = 16\,000$ and $\beta = 0$.

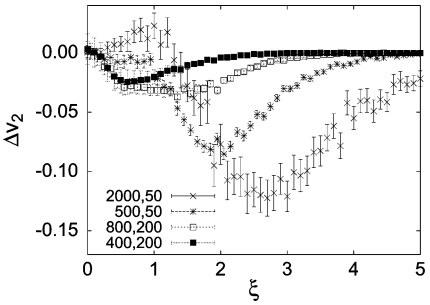

Figure 8. Results for $\Delta v_{2,\mathrm{opt}}(r;L_1,L_2)$ vs $\xi \equiv r/R_s$ for four different pairs of L_1 and L_2.

-1.8 for $\log \lambda = -3$, one obtains $a \approx 1.6$, that is still far from our estimate.

To determine the ξ dependence of $v_\infty(\xi;\lambda)$, we consider the rescaled quantity

$$\beta v_r(r;L_1,L_2;\beta) = \frac{\beta v(r;L_1,L_2;\beta)}{\beta v(0;L_1,L_2;\beta)} \tag{47}$$

In Figure 7 we report this function for $\beta = 0$, $L_1 = 16\,000$, and several values of L_2. On the scale of the figure, in the reported range $\xi \lesssim 1.5$, all data that correspond to different values of λ collapse on a single curve. Thus, we can write

$$v_\infty(\xi;\lambda) \approx v_{\mathrm{approx}}(\xi;\lambda) = v_\infty(\xi = 0;\lambda)\frac{v_\infty(\xi;1)}{v_\infty(0;1)} \tag{48}$$

and use the precise results of ref 18 for the effective pair potential $v_\infty(\xi;1)$ between two polymers of equal length. To identify the corrections, in Figure 8 we plot

$$\Delta v_2(r;L_1,L_2) = \beta v(r;L_1,L_2) - v_{\mathrm{approx}}(\xi;\lambda) \tag{49}$$

as a function of ξ, for the optimal combination. It is evident that corrections are tiny, except for λ small, say $\lambda \lesssim 0.1$, where approximation (48) significantly overestimates the pair potential in the region $\xi \approx 1-5$.

The coarse-graining procedure gives rise to higher order interactions beside the effective pair potential.[8] For small densities, the most relevant one is the three-body potential. We have computed this quantity for r_{12}, r_{13}, $r_{23} \lesssim 2R_s$ for the case $L_1 = L_2$ and a few values of L_1/L_3. The calculation is extremely CPU intensive, and thus, for each value of L_1/L_3 we have only considered one pair L_1, L_3. The longest walk has always $L = 2000$, while the shortest one has been chosen such as to obtain the appropriate length ratio. Without a proper extrapolation, data may be affected by corrections to scaling. To minimize them, we performed runs at $\beta = 0.054$, which is the value of β for which leading scaling corrections approximately cancel.[18] To verify the cancellation, we have computed the three-body potential for $r_{12} = r_{13} = r_{23} = 0$ also for a second set of walks in which the longest one has $L = 1000$. The results, reported in Table 1, show that scaling corrections are small compared with the error bars. In Figure 9 we give $\beta v_3(r, r, r; L_1, L_1, L_3; \beta = 0.054)$ for an equilateral configuration $r_{12} = r_{13} = r_{23} = r$. It is evident that the three-body interaction decreases as $L_1/L_3 \to 0$ or $L_1/L_3 \to \infty$, consistent with the idea that the effective potential goes to zero when the length of some of the walks is much smaller than the length of one of them. Qualitatively, the three-body potential shows the same behavior for all values of λ. It is always negative in the range $\xi \lesssim 2$, and $\beta v_3(0, 0, 0)/\beta v_2(r = 0)$ is approximately $-1/4$ in all cases. Only the range of the potential is slightly different. For $\lambda = 1$ it becomes essentially zero for $\xi \approx 1$, while for the other values of λ it vanishes approximately for $\xi \approx 1.5-2$.

Table 1. Three-Body Potential $\beta v_3(0,0,0;L_1,L_1,L_3;\beta)$ at Full Overlap for $\beta = 0.054$[a]

λ	L_1	L_3	βv_3
0.125	125	1000	−0.260(13)
0.125	250	2000	−0.256(10)
0.25	250	1000	−0.421(23)
0.25	500	2000	−0.364(15)
1	1000	1000	−0.478(13)
1	2000	2000	−0.464(10)
4	1000	250	−0.409(21)
4	2000	500	−0.384(13)
8	1000	125	−0.318(12)
8	2000	250	−0.305(9)

[a] Here $\lambda = L_1/L_3$. The number in parentheses gives the error on the last reported digits.

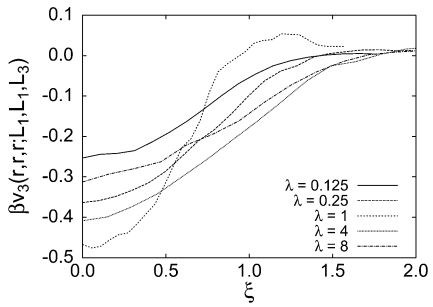

Figure 9. Results for $\beta v_3(r,r,r;L_1,L_1,L_3)$ as a function of $\xi \equiv r/R_s$. Here $\lambda = L_1/L_3$ and $\beta = 0.054$ (optimal β); the largest of the two lengths L_1 and L_3 is always $L = 2000$.

4. Osmotic Pressure and Structur Factor in the Dilute Limit

4.1. General Results. We now wish to use the results of section 3 to compute the osmotic pressure and the intermolecular structure function. In the scaling limit the osmotic pressure Π can be written as

$$\frac{\beta\Pi}{\rho} = f_\Pi(\rho R_{g,Z}{}^3) \tag{50}$$

where ρ is the polymer number density and $R_{g,Z}$ is the zero-density Z-averaged radius of gyration introduced in section 2. (This choice is motivated by convenience; any other quantity related to the size of the polymer would work equally well.) The scaling function $f_\Pi(x)$ depends on the polydispersity distribution but is independent of chemical details. For small x it behaves as $f_\Pi(x) = 1 + A_2^\Pi(P)x + O(x^2)$. Expression 50 may be experimentally inconvenient since it requires an independent determination of $R_{g,Z}$ at zero density. One can avoid the use of $R_{g,Z}$ by writing

$$\frac{\beta\Pi}{\rho} = \hat{f}_\Pi(\rho B_2^\Pi) \tag{51}$$

The function $\hat{f}_\Pi(x)$ is also independent of chemical details and is normalized so that $\hat{f}_\Pi(x) = 1 + x + O(x^2)$. In the following we shall report results in terms of ρB_2^Π but note that results in terms of $\rho R_{g,Z}{}^3$ can be obtained by using $\rho R_{g,Z}{}^3 = \rho B_2^\Pi / A_2^\Pi(P)$ and the results of section 3 for $A_2^\Pi(P)$.

In this paper we only discuss the dilute regime. For monodisperse systems it corresponds to densities $\rho \lesssim \rho^*$, where

$$\frac{1}{\rho^*} = \frac{4\pi}{3} R_g{}^3 \tag{52}$$

and R_g is the zero-density radius of gyration. In terms of $\rho B_2(L,L)$, $\rho \lesssim \rho^*$ corresponds to $\rho B_2(L,L) \lesssim 1.3$. Roughly speaking, the dilute regime corresponds to the range of densities in which the virial expansion holds. In the polydisperse case, especially if the distribution of sizes is broad, it is not clear how to characterize the dilute regime in terms of the size of the polymers. It is instead natural to identify it with the range in which $\rho B_2^\Pi \lesssim 1$.[32] This is the regime that will be considered below.

To determine the osmotic pressure as a function of ρ for a generic polydispersity distribution, we will use the coarse-grained potential derived in section 3; i.e., we schematize the polymer solution as a mixture of point particles distributed according to the polydispersity distribution and interacting by means of the zero-density coarse-grained potential. To determine the thermodynamic properties, we use the integral-equation formalism.[9] Given a mixture of M different species labeled by the index α (each species corresponds to polymers of length L_α), we define the direct correlation function $c_{\alpha\beta}(\mathbf{r})$ by the Ornstein−Zernike relation

$$\hat{h}_{\alpha\beta}(\mathbf{k}) = \hat{c}_{\alpha\beta}(\mathbf{k}) + \rho \sum_{\lambda=1}^{M} x_\lambda \hat{c}_{\alpha\lambda}(\mathbf{k})\, \hat{h}_{\lambda\beta}(\mathbf{k}) \tag{53}$$

where $h_{\alpha\beta}(\mathbf{r})$ is the pair correlation function, $\hat{h}_{\alpha\beta}(\mathbf{k})$ and $\hat{c}_{\alpha\beta}(\mathbf{k})$ are the corresponding Fourier transforms, ρ is the number density of the mixture, and x_α is the number fraction of the particles (polymers) of type α. To solve the thermodynamics, one needs a closure relation between $h_{\alpha\beta}(\mathbf{r})$ and $c_{\alpha\beta}(\mathbf{r})$. We will use the HNC closure

$$h_{\alpha\beta}(\mathbf{r}) + 1 = \exp[-\beta v_{\alpha\beta}(\mathbf{r}) + h_{\alpha\beta}(\mathbf{r}) - c_{\alpha\beta}(\mathbf{r})] \tag{54}$$

where $v_{\alpha\beta}(\mathbf{r})$ is the potential between particles of type α and β. In ref 10 it was shown that the HNC approximation is very accurate for soft-core potentials. The pressure may be computed either by using the virial equation

$$\frac{\beta\Pi}{\rho} = 1 - \frac{2\pi}{3}\rho \sum_{\alpha\beta} x_\alpha x_\beta \int_0^\infty \mathrm{d}r\, r^2 [r h_{\alpha\beta}(r) \beta v'_{\alpha\beta}(r) - 3\beta v_{\alpha\beta}(r)] \tag{55}$$

or by using the compressibility route, which requires the integration over density of the direct correlation function at fixed composition:

$$\frac{\beta\Pi}{\rho} = 1 - \frac{1}{\rho}\int_0^\rho \mathrm{d}\sigma\, \sigma \sum_{\alpha\beta} x_\alpha x_\beta \hat{c}_{\alpha\beta}(\mathbf{k}=0;\sigma) \tag{56}$$

Here $\hat{c}_{\alpha\beta}(\mathbf{k}=0;\sigma)$ is the zero-momentum direct correlation function at density σ. For soft-core potentials the two definitions give the same result, and thus the HNC closure provides a consistent thermodynamics. We have computed the pressure using both methods, verifying that they give the same value for Π. This provides a strong check of the correctness of our numerical programs.

Beside the osmotic pressure, we also compute the intermolecular structure factor defined by

$$S_{\mathrm{inter}}(\mathbf{q}) \equiv \frac{1}{V} \sum_{m\neq n} \sum_{a\in m} \sum_{b\in n} \langle \mathrm{e}^{i\mathbf{q}\cdot(\mathbf{r}_a^{(m)} - \mathbf{r}_b^{(n)})} \rangle \tag{57}$$

where V is the volume, m, n label the polymers, and a, b refer to the monomers that belong to polymers m and n. Within our coarse-grained model it is not possible to determine $S_{\mathrm{inter}}(\mathbf{q})$ exactly. In the monodisperse case, a precise approximation (at least for $qR_g \lesssim 8$) has been proposed in ref 33. Their approximation can be easily generalized to the polydisperse case (see Appendix). We first rewrite the intermolecular structure factor as (as usual, we neglect here end effects)

$$S_{\mathrm{inter}}(\mathbf{q}) = \rho^2 \sum_{\alpha\beta} x_\alpha x_\beta L_\alpha L_\beta \hat{h}_{\mathrm{mm},\alpha\beta}(\mathbf{q}) \tag{58}$$

where $\hat{h}_{\mathrm{mm},\alpha\beta}(\mathbf{q})$ is the monomer−monomer correlation function and x_α and L_α are respectively the number density and the length of polymers of type α. In the Appendix, generalizing the argument of ref 33, we relate the monomer−monomer correlation function to the correlation function between the centers of mass of the polymers $\hat{h}_{\alpha\beta}(\mathbf{q})$ computed in the coarse-grained model. This gives us the relation

$$S_{\mathrm{inter}}(\mathbf{q}) = \rho^2 \sum_{\alpha\beta} x_\alpha x_\beta L_\alpha L_\beta \frac{\omega_{\mathrm{mm}}^{(\alpha)}(\mathbf{q}) \omega_{\mathrm{mm}}^{(\beta)}(\mathbf{q})}{\omega_{\mathrm{cm}}^{(\alpha)}(\mathbf{q}) \omega_{\mathrm{cm}}^{(\beta)}(\mathbf{q})} \hat{h}_{\alpha\beta}(\mathbf{q}) \tag{59}$$

where $\omega_{\mathrm{mm}}^{(\alpha)}(\mathbf{q})$ and $\omega_{\mathrm{cm}}^{(\alpha)}(\mathbf{q})$ are form factors defined respectively as

$$\omega_{\mathrm{mm}}^{(\alpha)}(\mathbf{q}) \equiv \frac{1}{L_\alpha + 1} \sum_{a=0}^{L_\alpha} \sum_{b=0}^{L_\alpha} \langle \mathrm{e}^{i\mathbf{q}\cdot(\mathbf{r}_a - \mathbf{r}_b)} \rangle_\alpha \tag{60}$$

$$\omega_{\mathrm{cm}}^{(\alpha)}(\mathbf{q}) \equiv \sum_{a=0}^{L_\alpha} \langle e^{i\mathbf{q}\cdot(\mathbf{r}_a - \mathbf{r}_{\mathrm{CM}})} \rangle_\alpha \tag{61}$$

where $\langle\cdot\rangle_\alpha$ indicates the average over polymers of species α and $\mathbf{r}_{\mathrm{CM}}$ is the center-of-mass position. In ref 33 it was shown that a good approximation for q not too large, say $qR_g \lesssim 8$, is obtained by using the form factors valid for ideal polymers:[34]

$$\frac{1}{L_\alpha + 1}\omega_{\mathrm{mm}}^{(\alpha)}(\mathbf{q}) = \frac{2}{x^4}(\mathrm{e}^{-x^2} - 1 + x^2)$$

$$\frac{1}{L_\alpha + 1}\omega_{\mathrm{cm}}^{(\alpha)}(\mathbf{q}) = \frac{\sqrt{\pi}}{x}\mathrm{e}^{-x^2/12}\,\mathrm{erf}(x/2) \tag{62}$$

where $\mathrm{erf}(x)$ is the error function, $x = qR_{g,\alpha}$, and $R_{g,\alpha}$ is the radius of gyration of polymers of species α. Below, we will use eq 59 with the form factors (62) to compute the intermolecular structure factor.

In the scaling limit, the intermolecular structure function satisfies a scaling relation analogous to that of the pressure. Indeed, we have

$$\Sigma(\mathbf{q}) \equiv \frac{S_{\text{inter}}(\mathbf{q})}{\rho \sum_{\alpha} x_{\alpha} L_{\alpha}^2} = \hat{f}_S(qR_g,\rho R_g^3) = \hat{f}_S(qR_g,\rho B_2^{\Pi}) \quad (63)$$

It is easy to verify that the function $\hat{f}_S(qR_g,\rho B_2^{\Pi})$, which depends only on the polydispersity distribution, satisfies $\hat{f}_S(0,x) = -2B_2^S x/B_2^{\Pi}$ for $x \to 0$.

4.2. Bimodal Polydispersity. In this section we consider a ternary system in which there are two polymer species with the same chemical composition but with different degree of polymerization L_1 and L_2. As before, we set $\lambda \equiv L_2/L_1$ and indicate with $\alpha = x_1$ the number density of polymers of length L_1. In Figure 10 we report $Z \equiv \beta\Pi/\rho$ vs $\rho R_{g,Z}{}^3$ and ρB_2^{Π}. It is computed by using the HNC integral equations and the approximate potential (48). It is evident that ρB_2^{Π} is the most natural variable. Indeed, all mixtures have approximately the same Z at the same value of ρB_2^{Π}. Polydispersity is essentially encoded in the variable B_2^{Π}, the additional dependence being quite small. Note that this approximate independence is not trivially due to the fact that Z is well approximated by the first two terms of the virial expansion. As can be seen in Figure 10, Z is significantly different from $1 + \rho B_2^{\Pi}$. Note also that for large densities Z is approximately linear. As discussed in ref 10, this is a general result for soft-core potentials. Of course, in a polymer system this behavior holds only in some intermediate range of densities. As ρ increases, higher order interactions become important, and eventually Z scales as[1] $Z \sim r^{1/(3\nu-1)} \sim r^{1.311}$. In the intermediate linear regime, the pressure can be computed directly in the random-phase approximation, which corresponds to taking $c_{\alpha\beta}(\mathbf{r}) = -v_{\alpha\beta}(\mathbf{r})$. The pressure is then given by

$$\frac{\beta\Pi}{\rho} = 1 + \frac{\rho}{2}\sum_{\alpha\beta} x_{\alpha}x_{\beta}\int \mathrm{d}^3\mathbf{r}\, v_{\alpha\beta}(\mathbf{r})$$

$$= 1 + \frac{B_2^{\Pi}\rho}{2}\, v_p \frac{\alpha^2 + \beta^2\lambda^{3\nu} + 2\alpha\beta[(1+\lambda^2)/2]^{3\nu/2} v_{\infty}(0;\lambda)/v_{\infty}(0;1)}{(\alpha^2 + \beta^2\lambda^{3\nu})A_2{}^*(1) + 2\alpha\beta\lambda^{3\nu/2}A_2{}^*(\lambda)} \quad (64)$$

where

$$v_p = \int \mathrm{d}^3\mathbf{r}\, v_{\infty}(r;1) \approx 14.31 \quad (65)$$

To identify better the deviations from the monodisperse case, we consider

$$R(\lambda,\alpha,B_2^{\Pi}\rho) \equiv \left(\frac{\beta\Pi}{\rho} - 1\right)\frac{1}{B_2^{\Pi}\rho} \quad (66)$$

which satisfies

$$R(\lambda,0,x) = R(\lambda,1,x) = R_{\text{md}}(x) \quad (67)$$

$$R(\lambda,\alpha,x) = 1 + O(x) \qquad \text{for } x \to 0 \quad (68)$$

where $R_{\text{md}}(x)$ is the same quantity in a monodisperse system. In Figure 11 we report $R(\lambda,\alpha,x) - R_{\text{md}}(x)$, $x = B_2^{\Pi}\rho$, for $\lambda = 0.1$ and $\lambda = 0.5$. For $\lambda = 0.5$ differences between $R(\lambda,\alpha,x)$ and $R_{\text{md}}(x)$ are tiny. Their difference is zero for $\alpha = 0$, increases until $\alpha \approx 0.3$, and then decreases again. At $B_2^{\Pi}\rho = 1$ the difference is at most 0.007. For $\lambda = 0.1$ deviations are larger by approximately a factor of 10. The absolute difference of

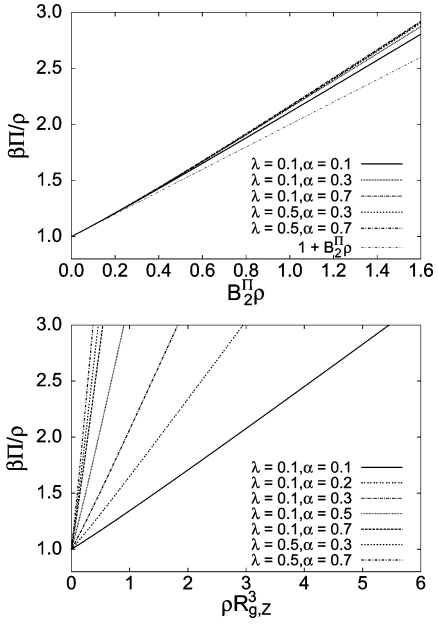

Figure 10. Pressure for bimodal solutions. Results for $\beta\Pi/\rho$ as a function of $B_2^{\Pi}\rho$ (top) and $\rho R_{g,Z}{}^3$ (bottom) for $\lambda = 0.1$, 0.5 and a few values of α. In the upper plot we also report (thin line) the approximation $\beta\Pi/\rho = 1 + B_2^{\Pi}\rho$.

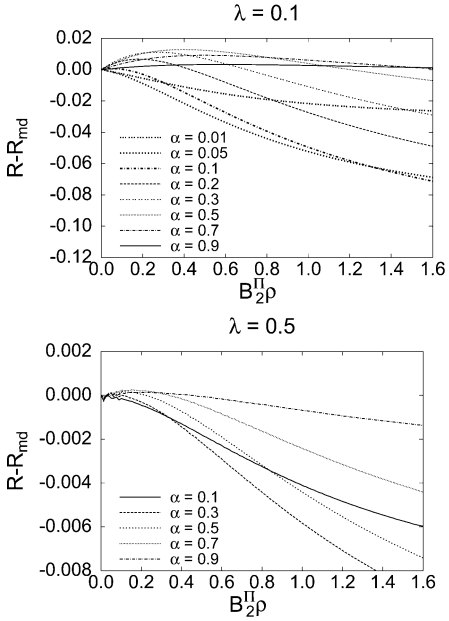

Figure 11. Pressure for bimodal solutions. Results for $R(\alpha,\lambda,x) - R_{\text{md}}(x)$ as a function of $x \equiv B_2^{\Pi}\rho$ for $\lambda = 0.1$ (top) and $\lambda = 0.5$ (bottom) and a few values of α.

$R(\lambda,\alpha,x)$ and $R_{\text{md}}(x)$ reported in the figure first increases rapidly with α, is maximal for $\alpha \approx 0.05$, and then slowly decreases toward zero as $\alpha \to 1$. Note that the rapid variation of R with α is similar to that observed in A_2^{Π} and A_2^S (see Figure 3). For small α the behavior of the solution is very sensitive to changes in the density of the (rare) long polymers. On the other hand, when α is close to 1, little changes when varying the density of the short polymers.

In ref 5 it was shown that the estimates of the pressure obtained by using the zero-density pair potential are lower than the correct result. This is due to the neglect of the three-body, four-body, etc., interactions. Their effect is not large in the dilute regime. Using the density-dependent potential reported in ref 35 and the HNC closure, we obtain that the correct pressure

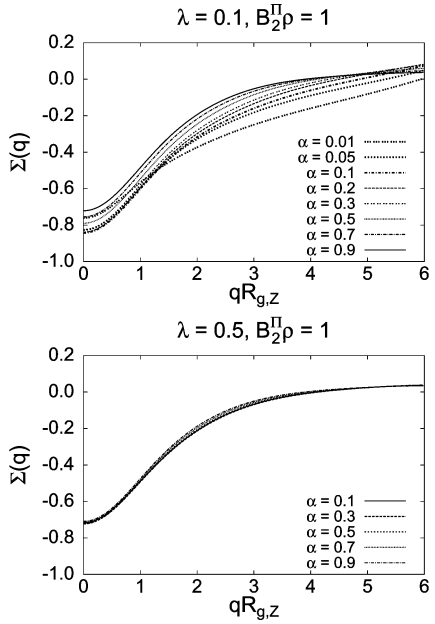

Figure 12. Intermolecular structure factor for bimodal solutions. Results for $\Sigma(\mathbf{q})$ as a function of $qR_{g,Z}$ at $B_2^{\Pi}\rho = 1$ for $\lambda = 0.1$ (top) and $\lambda = 0.5$ (bottom).

(computed by using the compressibility route, see ref 36) at $B_2\rho = 1$ for a monodisperse system is only 7% larger than that computed by using the zero-density potential. An analogous correction is expected in the presence of polydispersity.

We have also considered the intermolecular structure factor. The previous discussion indicates that a meaningful comparison should be done at fixed values of $B_2^{\Pi}\rho$. In Figure 12 we report the scaling function $\Sigma(\mathbf{q})$ for $B_2^{\Pi}\rho = 1$ as a function of $qR_{g,Z}$. For $\lambda = 0.5$ polydispersity effects are tiny and not visible on the scale of the figure. For $\lambda = 0.1$ the dependence on α is somewhat larger. For $\mathbf{q} = 0$, $\Sigma(0)$ first decreases abruptly, reaching a minimum for $\alpha \approx 0.05$, and then increases slowly again as α increases toward 1. This is very similar to what is observed for the pressure. For $\mathbf{q} \neq 0$, the behavior is similar: $\Sigma(\mathbf{q})$ first decreases, reaching a minimum at a q-dependent value $\alpha(q)$, and then increases again. Apparently, $\alpha(q)$ decreases as q increases: for $qR_g = 2$ (3) we have $\alpha(q) \approx 0.01$ (0.005). Note finally that $\Sigma(\mathbf{q}) \approx 0$ for $qR_{g,Z} \gtrsim Q_0$ with $Q_0 \approx 4$ for the monodisperse case. In the bimodal case, first Q_0 increases rapidly as α increases, until $\alpha \approx 0.005-0.01$, and then slowly decreases toward the monodisperse value $Q_0 \approx 4$.

For the monodisperse case, exact simulation results are reported in ref 33. Comparing with those obtained here for the monodisperse case, we see that the use of the zero-density pair potentials gives a quite good approximation. We expect therefore that also our polydispersity results in the dilute region are reasonably precise. In analogy with the discussion of the osmotic pressure, it is probably safe to assume that the error is less than 10%.

4.3. Schultz Distribution. The analysis of systems distributed according to the Schultz distribution is more complex since we are dealing with a continuous distribution of lengths. To perform the calculation, we work as follows. Given the polydispersity distribution $p(y)$ defined in eq 32, we first choose a number $\Lambda \ll 1$ and determine the interval $[y_1, y_2]$ such that $p(y) \geq \Lambda$ for $y_1 \leq y \leq y_2$ (for $\sigma \leq 1$ we have $y_1 = 0$). Then, we choose an integer M and define $\Delta y \equiv (y_2 - y_1)/M$. The polydisperse solution is approximated by a mixture of M different species, each species representing a polymer of different length. Species

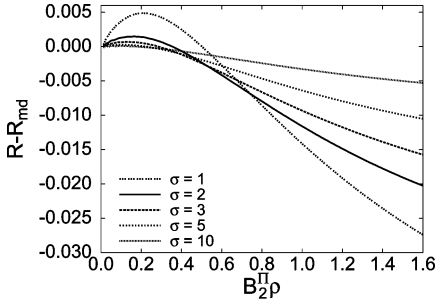

Figure 13. Osmotic pressure for the Schultz distribution. Results for $R(\sigma,x) - R_{md}(x)$ as a function of $x \equiv B_2^{\Pi}\rho$ for a few values of σ.

Table 2. Estimates of R (See Eq 66) for $\sigma = 1$ and $B_2^{\Pi}\rho = 1$, 1.5 for Several Values of the Parameters M, Λ, $\Delta r/R_{g,Z}$, and N_p

M	L	$\Delta r/R_{g,Z}$	N_p	$B_2^{\Pi}\rho = 1$	$B_2^{\Pi}\rho = 1.5$
25	10^{-3}	0.01	1024	1.1435	1.1664
50	10^{-3}	0.01	1024	1.1448	1.1678
100	10^{-3}	0.01	1024	1.1453	1.1682
25	10^{-4}	0.005	2048	1.1418	1.1646
25	10^{-4}	0.01	4096	1.1419	1.1646
25	10^{-4}	0.02	1024	1.1419	1.1646
50	10^{-4}	0.02	1024	1.1439	1.1667
100	10^{-4}	0.02	1024	1.1445	1.1674

α, $1 \leq \alpha \leq M$, corresponds to polymers of length

$$\frac{L_\alpha}{N} = y_1 + \Delta y\left(\alpha - \frac{1}{2}\right) \tag{69}$$

The corresponding number fraction is

$$x_\alpha = \frac{1}{K}\int_{y_\alpha^-}^{y_\alpha^+} p(y)\, dy, \quad y_\alpha^{\pm} = \frac{L_\alpha}{N} \pm \frac{\Delta y}{2} \tag{70}$$

where K is a normalization factor ensuring $\sum x_\alpha = 1$. The continuous distribution results are obtained for $\Lambda \to 0$ and $M \to \infty$. Since we are dealing with a broad distribution of lengths, one should also carefully check the grid size $\Delta r/R_{g,Z}$ and the number of points N_p used in the solution of the integral equations. Values of the variable R defined in eq 66 are reported in Table 2 for $\sigma = 1$, $B_2^{\Pi}\rho = 1$, 1.5, and several values of the parameters. It is clear that $N_p = 1024$, $\Delta r/R_{g,Z} = 0.02$, $M = 100$, $\Lambda = 10^{-4}$ is fully adequate. The dependence on M and Λ decreases with increasing σ, and for $\sigma = 10$ we obtain $R = 1.1554$ ($B_2^{\Pi}\rho = 1$) and $R = 1.1880$ ($B_2^{\Pi}\rho = 1.5$) for all values of the parameters used in Table 2. In the following we shall report results obtained by using $M = 100$ and $\Lambda = 10^{-4}$. The discrete distribution obtained for such values of the parameters gives a very precise approximation of the continuous polydispersity distribution.

In Figure 13 we report R, as defined in eq 66, for several values of σ. The dependence on σ is tiny, and for $\sigma \gtrsim 5$, results cannot be distinguished from those of a monodisperse system. In Figure 14 we give the intermolecular structure function $\Sigma(\mathbf{q})$ for several values of $B_2^{\Pi}\rho$ and $qR_{g,Z}$. Also in this case the dependence on σ is small.

5. Conclusions

In this paper we have studied the effect of polydispersity on the behavior of polymer solutions in the good-solvent regime. First, we have focused on the second virial coefficient and on the effective pair potential between the centers of mass of two polymers of length L_1 and L_2. Results are given for systems in which polymers of two different lengths are present and for systems in which the polydispersity distribution follows the

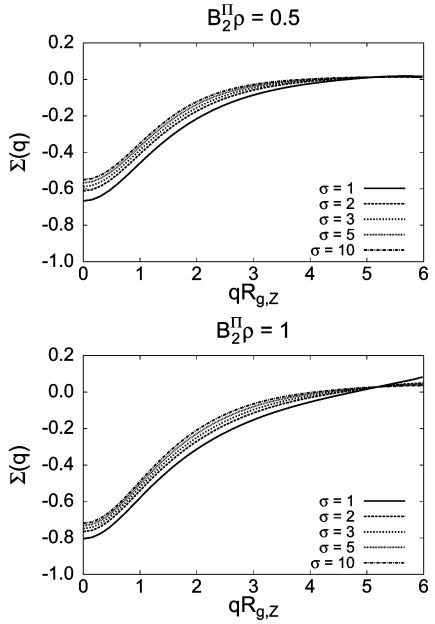

Figure 14. Intermolecular structure function for the Schultz distribution. Results for $\Sigma(\mathbf{q})$ as a function of $qR_{g,Z}$ at $B_2^\Pi\rho = 0.5$ (top) and $B_2^\Pi\rho = 1$ (bottom) for several values of σ.

Schultz law. Knowledge of the effective pair potential allows us to determine the osmotic pressure and the intermolecular structure factor in the dilute regime. We show that the natural variable is $B_2^\Pi\rho$ (or equivalently the dimensionless quantity $M_n B_{2,expt}^\Pi\rho_w$): systems with different polydispersity distributions have approximately the same $\beta\Pi/\rho$ at the *same* value of $B_2^\Pi\rho$. In particular, the dependence on the Schultz parameter is tiny, and for $\sigma \gtrsim 5$, the behavior of $\beta\Pi/\rho$ as a function of $B_2^\Pi\rho$ is practically equal to that occurring in a monodisperse system. We have also computed the intermolecular structure function generalizing the results of ref 33 to a polydisperse system. Again, polydispersity effects are small when one compares the structure functions at the same value of $B_2^\Pi\rho$.

All the considerations presented here apply to the good-solvent regime, and thus our results are only predictive far from the θ point. Approaching the θ point significant deviations occur. A proper parametrization of this crossover, along the lines discussed in ref 18, will be presented in a forthcoming publication.

Finally, we should mention that our results also apply to solutions of polymers of different chemical composition. Indeed, as discussed in refs 3, 24, 37, and 38, the difference in the nature of the polymers gives rise to new scaling corrections (see ref 39 for a precise numerical determination) but does not change the universal behavior in the scaling limit. To apply the present results to multicomponent solutions, one should realize that the degree of polymerization is not a meaningful variable in the presence of polymers of different chemical composition. In this case the size of the polymers should be characterized by using, e.g., the radius of gyration. In practice, given a solution with several species, $1 \le \alpha \le M$, with zero-density radii of gyration $R_{g,\alpha}$, one can define *effective* lengths

$$L_\alpha = R_{g,\alpha}{}^{1/\nu} \tag{71}$$

In the scaling limit, the multicomponent solution behaves as a polydisperse solution of polymers of length L_α. It is important to note that scaling corrections are particularly strong (see ref 39), and thus, even with long polymers, we expect sizable deviations from the scaling limit determined here.

Acknowledgment. The author thanks Jean-Pierre Hansen for useful discussions and suggestions.

Appendix. A PRISM Approximation for the Monomer−Monomer Correlation Function

To compute the intermolecular structure function, we need to relate the monomer−monomer correlation function to the coarse-grained correlation $\hat{h}_{\alpha\beta}(\mathbf{q})$. We will generalize here the expression obtained in ref 33 for monodisperse systems. For convenience, we relabel $\hat{h}_{\alpha\beta}(\mathbf{q})$ as $\hat{h}_{cc,\alpha\beta}(\mathbf{q})$ to emphasize that it corresponds to the center-of-mass−center-of-mass correlation function. Then, we introduce the center-of-mass−monomer correlation function $\hat{h}_{cm,\alpha\beta}(\mathbf{q})$, the corresponding direct correlation functions, and assume, as in ref 33, that only the monomer−monomer direct correlation function $\hat{c}_{mm,\alpha\beta}(\mathbf{q})$ is nonvanishing. Then, we consider the PRISM Ornstein−Zernike[40] relation. With the above-reported assumption on the direct correlation functions, we can write

$$\hat{h}_{ab,\alpha\beta} = \omega_{am}^{(\alpha)}\hat{c}_{mm,\alpha\beta}\omega_{bm}^{(\beta)} + \rho\sum_\gamma \omega_{am}^{(\alpha)}\hat{c}_{mm,\alpha\gamma}x_\gamma L_\gamma \hat{h}_{mb,\gamma\beta} \tag{72}$$

where a and b may be either m or c, and $\omega_{bm}^{(\alpha)}$ are the polymer form factors defined in section 4.1. All functions depend on the wave vector $\mathbf{q}$ that has not been explicitly written. Then, define

$$H_{ab,\alpha\beta} \equiv \frac{\omega_{mm}^{(\alpha)}\omega_{mm}^{(\beta)}}{\omega_{am}^{(\alpha)}\omega_{bm}^{(\beta)}}\hat{h}_{ab,\alpha\beta} \tag{73}$$

Equation 72 implies

$$H_{ab,\alpha\beta} = \omega_{mm}^{(\alpha)}\hat{c}_{mm,\alpha\beta}\omega_{mm}^{(\beta)} + \rho\sum_\gamma \omega_{mm}^{(\alpha)}\hat{c}_{mm,\alpha\gamma}x_\gamma L_\gamma H_{mb,\gamma\beta} \tag{74}$$

Then, we obtain

$$H_{ab,\alpha\beta} - H_{mm,\alpha\beta} = \rho\sum_\gamma \omega_{mm}^{(\alpha)}\hat{c}_{mm,\alpha\gamma}x_\gamma L_\gamma (H_{mb,\gamma\beta} - H_{mm,\gamma\beta}) \tag{75}$$

This set of equations is solved by taking

$$H_{ab,\alpha\beta} = H_{mm,\alpha\beta} \tag{76}$$

which implies

$$\hat{h}_{mm,\alpha\beta} = \frac{\omega_{mm}^{(\alpha)}\omega_{mm}^{(\beta)}}{\omega_{am}^{(\alpha)}\omega_{bm}^{(\beta)}}\hat{h}_{ab,\alpha\beta} \tag{77}$$

References and Notes

(1) de Gennes, P. G. *Scaling Concepts in Polymer Physics*; Cornell University Press: Ithaca, NY, 1979.
(2) Freed, K. F. *Renormalization Group Theory of Macromolecules*; Wiley: New York, 1987.
(3) Schäfer, L. *Excluded Volume Effects in Polymer Solutions*; Springer: Berlin, 1999.
(4) At present the most accurate estimates of ν are $\nu = 0.58758 \pm 0.00007$ [ref 17], $\nu = 0.5874 \pm 0.0002$ [Prellberg, T. *J. Phys. A: Math. Gen.* **2001**, *34*, L599−L602], $\nu = 0.58765 \pm 0.00020$ [Hsu, H.-P.; Nadler, W.; Grassberger, P. *Macromolecules* **2004**, *37*, 4658−4663]. For an extensive list of results, see: Pelissetto, A.; Vicari, E. *Phys. Rep.* **2002**, *368*, 549−727.
(5) Bolhuis, P. G.; Louis, A. A.; Hansen, J. P.; Meijer, E. J. *J. Chem. Phys.* **2001**, *114*, 4296−4311.

(6) Grosberg, A. Y.; Khalatur, P. G.; Khokhlov, A. R. *Makromol. Chem. Rapid Commun.* **1982**, *3*, 709−713.
(7) Hansen, J. P.; Addison, C. I.; Louis, A. A. *J. Phys.: Condens. Matter* **2005**, *17*, S3185−S3193.
(8) Bolhuis, P. G.; Louis, A. A.; Hansen, J. P. *Phys. Rev. E* **2001**, *64*, 021801.
(9) Hansen, J.-P.; McDonald, I. R. *Theory of Simple Liquids*, 2nd ed.; Academic: London, 1986.
(10) Louis, A. A.; Bolhuis, P. G.; Hansen, J. P. *Phys. Rev. E* **2000**, *62*, 7961−7972.
(11) Grassberger, P.; Hegger, R. *J. Chem. Phys.* **1995**, *102*, 6881−6899. Grassberger, P. *Phys. Rev. E* **1997**, *56*, 3682−3693.
(12) Lal, M. *Mol. Phys.* **1969**, *17*, 57−64.
(13) MacDonald, B.; Jan, N.; Hunter, D. L.; Steinitz, M. O. *J. Phys. A: Math. Gen.* **1985**, *18*, 2627−2631.
(14) Madras, N.; Sokal, A. D. *J. Stat. Phys.* **1988**, *50*, 109−186.
(15) Sokal, A. D. In *Monte Carlo and Molecular Dynamics Simulations in Polymer Science*; Binder, K., Ed.; Oxford University Press: Oxford, 1995.
(16) Muthukumar, M.; Nickel, B. G. *J. Chem. Phys.* **1987**, *86*, 460−476.
(17) Belohorec, P.; Nickel, B. G. *Accurate universal and two-parameter model results from a Monte-Carlo renormalization group study*; Guelph University report, 1997, unpublished.
(18) Pelissetto, A.; Hansen, J. P. *J. Chem. Phys.* **2005**, *122*, 134904.
(19) de Gennes, P. G. Talk cited in ref 23.
(20) Yamakawa, H. *Modern Theory of Polymer Solutions*; Harper-Row: New York, 1971.
(21) Lapp, A.; Mottin, M.; Strazielle, C.; Broseta, D.; Leibler, L. *J. Phys., II* **1992**, *2*, 1247−1256.
(22) Li, B.; Madras, N.; Sokal, A. D. *J. Stat. Phys.* **1995**, *80*, 661−754.
(23) Witten, T. A.; Prentis, J. J. *J. Chem. Phys.* **1982**, *77*, 4247−4253.
(24) Joanny, J. F.; Leibler, L.; Ball, R. *J. Chem. Phys.* **1984**, *81*, 4640−4656.
(25) Grassberger, P.; Sutter, P.; Schäfer, L. *J. Phys. A: Math. Gen.* **1997**, *30*, 7039−7056.
(26) Caracciolo, S.; Causo, M. S.; Pelissetto, A. *Phys. Rev. E* **1998**, *57*, R1215−R1218.
(27) Nickel, B. G. *Physica A* **1991**, *177*, 189−196. Murray, D. B.; Nickel, B. G. *Revised estimates for critical exponents for the continuum n-vector model in three dimensions*; Guelph University report, 1991, unpublished.
(28) Pelissetto, A.; Vicari, E. *Nucl. Phys. B* **1998**, *519*, 626−660.
(29) Pelissetto, A.; Vicari, E. *Nucl. Phys. B* **2000**, *575*, 579−598.
(30) Guida, R.; Zinn-Justin, J. *J. Phys. A: Math. Gen.* **1998**, *31*, 8103−8121.
(31) Krüger, B.; Schäfer, L.; Baumgärtner, A. *J. Phys. (Paris)* **1989**, *50*, 3191−3222.
(32) Of course, we are not claiming here that $B_2^{\Pi}\rho = 1$ is the radius of convergence of the virial expansion. What we mean is that the virial expansion is expected to converge up to $B_2^{\Pi}\rho$ of order 1.
(33) Krakoviack, V.; Hansen, J. P.; Louis, A. A. *Europhys. Lett.* **2002**, *58*, 53−59.
(34) Krakoviack, V.; Rotenberg, B.; Hansen, J. P. *J. Phys. Chem. B* **2004**, *108*, 6697−6706.
(35) Bolhuis, P. G.; Louis, A. A. *Macromolecules* **2002**, *35*, 1860−1869.
(36) Louis, A. A. *J. Phys.: Condens. Matter* **2002**, *14*, 9187−9206.
(37) Schäfer, L.; Kappeler, C. *J. Phys. (Paris)* **1985**, *46*, 1853−1864.
(38) Schäfer, L.; Lehr, U.; Kappeler, C. *J. Phys., I* **1991**, *1*, 211−233.
(39) Pelissetto, A.; Vicari, E. *Phys. Rev. E* **2006**, *73*, in press.
(40) Schweizer, K. S.; Curro, J. G. Integral Equation Theories of the Structure, Thermodynamics, and Phase Transitions in Polymer Fluids. In *Advances in Chemical Physics*; Prigogine, I., Rice, S. A., Eds.; Wiley: New York, 1997; Vol. XCVIII.

MA060250L